Two-Degrees-of-Freedom Controller delivering zero-error tracking of ramp-like trajectories for nanopositioning systems

Andres San-Millan[1], Sumeet S. Aphale[2] and Vicente Feliu[1]

Abstract— **Piezoelectrically actuated nanopositioning systems (tube or platform type) are widely employed in applications where fine mechanical displacements with resolution down to atomic scale are required. This paper presents the design, analysis, and validation of a new control scheme based on the structure of the traditional Two-Degrees-of-Freedom (2DOF) PID controller. The proposed controller is established based on a linear continuous input-output nominal model, and presents a simple structure composed by two second order transfer functions. Despite its simplicity, the controller studied in this paper is able to achieve zero error in the tracking of ramp and triangular input signals, typically used in nanopositioning applications to trace a raster pattern. The controller also suppresses the unmodeled nonlinearities of the piezoelectric actuated nanopositioning systems without the need of an hysteresis model or a state observer. Moreover, the stability of the control system is proved, and its effectiveness is validated through experimental chattering-free control on a piezoelectric stack-actuated nanopositioning platform. Results demonstrate that the proposed controller is superior to the conventional polynomial-based, proportional-integral, and resonant controllers proposed in literature for motion-tracking tasks in nanopositioning systems.**

I. INTRODUCTION

Micro-/nanopositioning has become key enabling technology in the field of biotechnology, fiber optics and atomic force microscopy (AFM). Several actuation mechanisms have been proposed for these precision positioning systems viz: electromagnetic motors, electrothermal actuators, electrostatic actuators, and piezoelectric actuators (PEAs). PEAs have been extensively utilized in micro-/nanopositioning applications because of their arbitrarily fine resolution (usually in the range of a nanometer)[1], high bandwidth, high force density, and absence of backlash and stickslip motion (due to an absence of any moving parts). Among the different PEA-driven nanopositioners available, flexure-based nanopositioners are beginning to replace the traditionally popular piezoelectric tube scanners due to their several advantages, namely: low cross-coupling between motion axes, robust mechanical construction, large motion range and high mechanical bandwidth, [2].

[1]A. San-Millan and V. Feliu are with the Universidad de Castilla-La Mancha, Ciudad Real 13071, Spain (e-mail: andres.sanmillan@uclm.es; vicente.feliu@uclm.es)

[2] Sumeet S. Aphale is with the Center for Applied Dynamics Research, School of Engineering, University of Aberdeen, Aberdeen, AB24 3UE, U.K. (e-mail:s.aphale@abdn.ac.uk)

However, flexure-based mechanisms exhibit two main dynamic characteristics that degrade their overall positioning performance: 1) nonlinear behaviour of piezoelectric actuators, such as hysteresis and creep, and 2)lightly damped resonant peaks of the flexible compliant mechanism, which impose an upper bound to the achievable bandwidth, determined by the first resonant mode of the nanopositioner [2]. The key challenges to achieve fast and precise positioning at these nanometer ranges are the compensation of the nonlinear behaviour and the damping of the first dominant resonant mode of the system. Though it is unclear as to whether linear controllers are actually capable of compensating for the nonlinear behaviour of the PEAs (hysteresis and creep), numerous works have experimentally shown that integral tracking control reduces the positioning error due to these nonlinearities and has thus become the most common method to improve positioning accuracy [3]. The main advantage of this approach is its simplicity and its independence from the requirement of an explicit hysteresis model.

On the other hand, several closed-loop damping control methodologies have been proposed to damping the first resonant mode of the system, thereby increasing the achievable positioning bandwidth of the positioner when used in tandem with a suitably gained integral tracking controller. Recent examples include robust control [4], sliding-mode control (SMC) [5], integral resonant control (IRC) [6], positive position feedback (PPF) [7], and polynomial-based control (also known as Positive Velocity and Position Feedback - PVPF) [8]. Thus, the simultaneous application of damping and tracking controllers to achieve high positioning performance is gaining popularity, [9]. Yet, it should be noted that as the typical input signals are triangular or ramp-like, a simple integral controller is incapable of delivering zero-error tracking performance. For zero-error tracking of such steadily increasing or decreasing trajectories, a double integral action is needed.

In this paper, a new control scheme, namely, two-degree of freedom PIID controller (2DOF-PI^{2}D) is proposed for micro-/nanopositioning applications. The presented controller can achieve an accurate positioning by compensating the nonlinear effects of the hysteresis without the utilisation of an explicit model of the hysteresis. The control scheme is therefore, extremely simple and consists of two nested control loops composed of second-order transfer functions. The proposed controller can also achieve zero-error tracking of ramp and triangular reference input signals. The ability of tracking ramp and triangular signals without steady error is of utmost benefit, since these signals are widely utilised in

atomic force microscopes (AFM) where raster scanning usually involves actuating one of the axes of the nanopositioner with a triangular signal and the other with a slow moving ramp. It is important also to note that the zero-error tracking has not been achieved yet by any of the previously proposed closed-loop control methodologies.

This paper is organized as follows. Section II presents the linear mathematical model of the piezo-actuated nanopositioner. Section III describes the design of the proposed 2DOF-PI^{2}D controller. Section IV details the experimental nanopositioning setup and the procedure utilised to identify its transfer function. An overview of the traditional control schemes is presented in Section V, and simulations are provided to evaluate the performance of the proposed controller in comparison with these traditional control schemes. Section VI presents the experimental results for the 2DOF-PI^{2}D controller, showing its effectiveness compared with the traditional designs in order to remove the tracking error of ramp and triangular signals. Section VII concludes the paper.

II. Problem formulation

A flexure-based nanopositioner can be interpreted as linear time-invariant Multiple-input Multiple-output (MIMO) system. Since most XY nanopositioners are designed to exhibit minimum cross-coupling between the two axes of motion (X and Y), the transfer-function matrix which relates the inputs and the outputs is diagonal. Thus, each axis of motion can be treated independently, exhibiting dynamics that can be represented by the following expression:

$$y_i(s) = g_i(s)u_i(s) + f_i(s); i = 1; 2 \qquad (1)$$

where $u_i(s)$ and $y_i(s)$ denote the Laplace transforms of the input and output of the system, $g_i(s)$ is the input-output transfer function, and $f_i(s)$ is the Laplace transform of the perturbation (which describes the combined effects of unmodeled nonlinear behaviour, and external perturbations), the subscript i represents each axis of motion ($i = [1; 2]$ for XY positioners). It is important to note that the input to the system, $u_i(s)$, is the voltage signal applied to the PEAs that moves the nanopositioner along each direction, and the output of the system, $y_i(s)$, corresponds to the voltage signals read by the sensors (usually a capacitive displacement sensor).

The transfer function which relates the input and the output of the system, $g_i(s)$ can be represented by means of an infinite sum of second-order transfer-functions as follows:

$$g_i(s) = \sum_{j=1}^{M} \frac{\frac{2}{j}}{s^2 + 2_j!_j s + !_j^2} \qquad (2)$$

where M $!$ 1, $\frac{2}{j}$ correspond to the gain of each mode of vibration, $_j$ is the damping ratio of each mode, and $!_j$ is the natural frequency of vibration of each mode. In order to reduce the complexity of model (2), it is usually truncated to a finite number of modes. In several works [9], [10], (2) is truncated to the first mode as it dominates over the
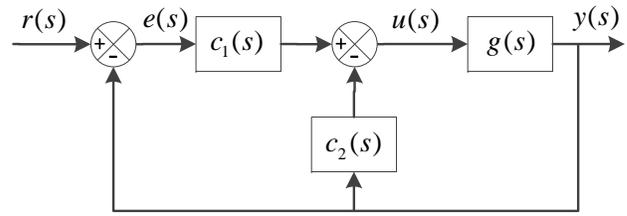

Fig. 1. 2DOF PID Control scheme

entire range of frequencies. The mathematical model of the nanopositioner can therefore be simplified to the following expression:

$$y_i(s) = \frac{2}{s^2 + 2_!s + !^2}u_i(s) + f_i(s) \qquad (3)$$

where only the first resonant mode is modelled.

Since the dynamics of the axes of motion are decoupled, the subscript i is hereafter omitted as the results obtained for the control of one axis of motion can be applied directly to the other.

III. 2DOF-PI^{2}D Desgin

As mentioned earlier, despite the presence of nonlinearities in the system, several linear closed-loop control schemes have already been proposed. According to [11], these control schemes are fixed-structure, low-order control laws composed of two sub-schemes: on the one hand, there is a sub-scheme responsible for imparting adequate damping to the first resonant mode of the system (in the form of positive position feedback, integral resonant control, integral force feedback, or passive shunt-damping) and, on the order hand, there is an integral control law which improves the reference tracking performance.

Since the integral control law is composed of a single integrator, these controllers can only track step signals without steady error, and when they are utilised to track ramp or triangular signals, they exhibit a constant tracking error. The control scheme proposed in this work is based on the 2DOFPID controller [12] shown in Fig. 1, where $g(s)$ is the transfer function of the nanopositioner, and $c_1(s)$ and $c_2(s)$ are the two transfer functions which combine to form the control scheme. In this figure, $r(s)$, $e(s)$, $u(s)$, and $y(s)$, are the reference applied to the system, the error signal, the voltage applied to the plant, and the output of the system respectively.

In order to achieve zero steady error when tracking a ramp signal, we propose transfer functions for the control scheme having the following structure:

$$c_1(s) = \frac{N_{11}s + N_{10}}{s^2} \qquad (4)$$

$$c_2(s) = \frac{N_{21}s + N_{20}}{s^2 + sD_{21} + D_{20}}; \qquad (5)$$

where $c_1(s)$ is composed of a double integrator, that allows to track ramp and triangular signals without any steady state error.

From Fig. 1 and the structure of the controller (4) (5), the closed-loop transfer function of the whole system is derived as:

$$
\begin{aligned}
g_{cl}^{num}(s) =\ & s^3\ {}^2 N_{11} + s^2\ {}^2(N_{11}D_{21} + N_{10}) \\
& + s\ {}^2(N_{11}D_{20} + N_{10}D_{21}) +\ {}^2 N_{10}D_{20} \\
g_{cl}^{den}(s) =\ & s^6 + s^5(2\ ! + D_{21}) \\
& + s^4(!\,^2 + 2\ D_{21}! + D_{20}) \\
& + s^3((N_{21} + N_{11}) + D_{21}!\,^2 + 2\ D_{20}!) \\
& + s^2(\ {}^2(N_{11}D_{21} + N_{20} + N_{10}) + D_{20}!\,^2) \\
& + s\ {}^2(N_{11}D_{20} + N_{10}D_{21}) \\
& +\ {}^2 N_{10}D_{20}
\end{aligned} \tag{6}
$$

where g_{cl}^{num} denotes the numerator, and g_{cl}^{den} the denominator, of the closed-loop transfer function. Applying the final value theorem to this equation, it can be seen that the steady state error when tracking ramp references is equal to zero. It can be seen from expression (6) that the closed-loop transfer function presents six poles which can be arbitrarily placed, since there are six parameters in the proposed controller which can be freely designed. In order to establish the relationship between the pole placement and the parameters of the controller and, therefore, the design equations, we can express the closed-loop characteristic equation in the form:

$$
s^6 + K_5 s^5 + K_4 s^4 + K_3 s^3 + K_2 s^2 + K_1 s + K_0 = 0; \tag{7}
$$

where:

$$
\begin{aligned}
K_5 =\ & (2\ ! + D_{21}) \\
K_4 =\ & (!\,^2 + 2\ D_{21}! + D_{20}) \\
K_3 =\ & ((N_{21} + N_{11}) + D_{21}!\,^2 + 2\ D_{20}!) \\
K_2 =\ & (\ {}^2(N_{11}D_{21} + N_{20} + N_{10}) + D_{20}!\,^2) \\
K_1 =\ & {}^2(N_{11}D_{20} + N_{10}D_{21}) \\
K_0 =\ & {}^2 N_{10}D_{20}
\end{aligned} \tag{8}
$$

Assuming a desired closed-loop characteristic equation (i.e. desired closed-loop poles), the parameters of the proposed controller can be designed by applying the following sequence of operations, where K_i is known as well as , ! and :

$$
\begin{aligned}
D_{21} =\ & K_5\quad 2\ ! \\
D_{20} =\ & K_4\quad !\,^2\quad 2\ !\,D_{21} \\
N_{10} =\ & K_0{=}(\ {}^2 D_{20}) \\
N_{11} =\ & (K_1\quad {}^2 D_{21}N_{10}){=}(\ {}^2 D_{20}) \\
N_{20} =\ & (K_2\quad D_{20}!\,^2\quad (D_{21}N_{11} + N_{10})\ {}^2){=}\ {}^2 \\
N_{21} =\ & (K_3\quad D_{21}!\,^2\quad 2\ D_{20}!\quad N_{11}\ {}^2){=}\ {}^2
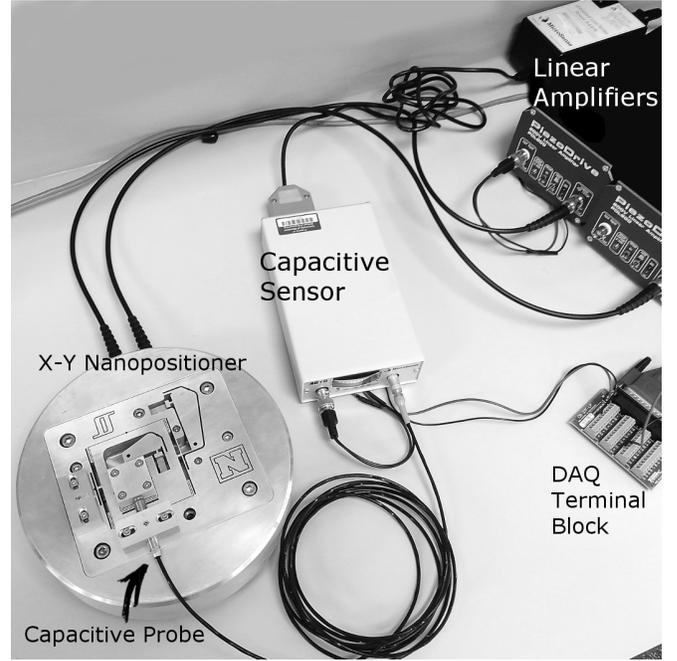\end{aligned} \tag{9}
$$

Fig. 2. Experimental setup used to verify the proposed control scheme.

These relationships will be used to design the controller transfer functions. The simulation and experimental results are presented in sections V and VI. The following section first describes the experimental setup utilized.

IV. EXPERIMENTAL SETUP

The performance of the proposed control scheme is evaluated on a two-axis serial kinematic nanopositioner, shown in Fig. 2. The nanopositioner, designed at the EasyLab, University of Nevada, Reno, USA , is actuated by two 10 mm 200 V piezoelectric stack actuators, driven by two low-noise, linear voltage amplifiers (PDL200) from Piezodrive, with an output range of [0, 200] V and a voltage gain of 20. The displacement of the nanopositioner is measured by a Microsense 6810 capacitive sensor and 6504-01 probe with a sensitivity of 5 m/V. The control algorithm is implemented using NI LabVIEWs Real-Time module at a sampling rate of 20 kHz.

A. System Identification

To identify the model of the plant, small signal frequency response functions (FRFs) were recorded. The FRFs were determined by applying a sinusoidal chirp (from 10 to 1000 Hz) with an amplitude of 0.2 Volts as input to the voltage amplifier of the x-axis and measuring the output signal in the same axis. Subsequently, the FRFs was computed by taking the Fourier transform of the recorded data. It should be noted that, using small amplitudes, the nonlinear effects of the PEAs such as hysteresis can be considered negligible. The magnitude and phase responses of the FRF of G(s) are plotted in Fig. 3.

The transfer function of the system was obtained by using the subspace based modelling technique described in [13] in
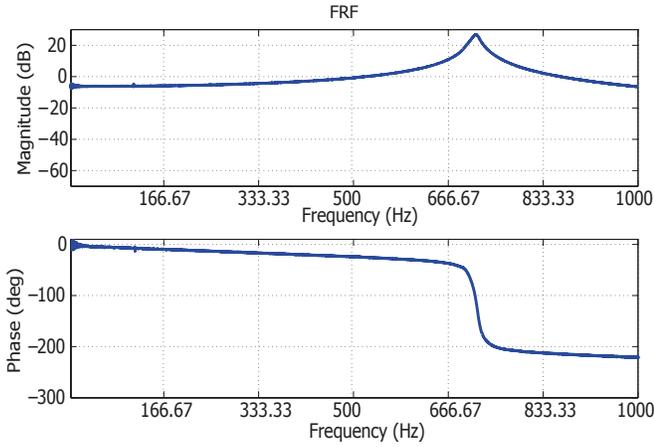
Fig. 3. Magnitude an Phase response of on axis of the nanopositioning platform.

order to identify the main resonant mode of the experimental platform. The identified model of the system is given by:

$$G(s) = \frac{1.024 \times 10^7}{s^2 + 99s + 2.025 \times 10^7} \quad (10)$$

The simulations presented in the following section were based on this identified transfer function.

V. SIMULATIONS

This section presents a comparison between the simulated results obtained by applying the proposed control scheme and three popular control schemes typically applied to nanopositioners, namely PPF, PVPF and IRC. Since the aim of this work is to present an effective, yet simple control scheme, the performance comparison is focused in the aforementioned controllers due to their simple design and superior performance. These control schemes are based on the block structures showed in Fig. 4 and are composed of low-order transfer functions.

The IRC controller is composed of first-order transfer functions of the form:

$$C_t(s) = \frac{k_t}{s} \quad (11)$$

$$C_d(s) = \frac{k_d}{s} \quad (12)$$

where k_t, k_d, and the constant gain d are the design parameters of the controller. The PPF, and PVPF designs are second-order of the form:

$$C_{dPPF}(s) = \frac{1}{s^2 + 2\zeta_c \omega_c s + \omega_c^2} \quad (13)$$

for the PPF, and:

$$C_{dPVPF}(s) = \frac{\gamma_2 s + \gamma_1}{s^2 + 2\zeta_c \omega_c s + \omega_c^2} \quad (14)$$

for the PVPF. In these expressions k_t, γ_1, γ_2, ζ_c, and ω_c are the parameters of the controllers to be chosen. All the

three controllers are then implemented as the inner (damping) loop controllers and an outer loop incorporating a tracking controller C_t, typically a suitable gained integrator is implemented simultaneously. It was shown in [11] that by using Model Reference Control to obtain a closed-loop Butterworth filter pattern (maximally flat magnitude response), an increased performance over traditional damping and tracking controllers is achieved in terms of bandwidth and positioning error. Moreover, in [14], explicit expressions to tune the three aforementioned controllers in order to obtain a closed-loop Butterworth filter pattern have been presented. In order to illustrate the better performance of the proposed controller compared with these three classic controllers (IRC, PPF, and PVPF) they have been designed by following the equations provided in [14] in order to compare the best results achievable. It is important to note that, according to (9), the closed-loop poles of the 2DOF-PI^{2}D controller proposed in this article can be arbitrarily placed. Thus parameters are chosen such that a Butterworth filter pattern is obtained for proposed the 2DOF-PI^{2}D controller, thereby allowing comparison of control schemes tuned using the same design methodolgy.

A. IRC Control scheme

By following the equations of design for the IRC control scheme shown in [14], the closed-loop poles of the system can be placed in a fourth-order Butterworth filter pattern, designing both the damping and the tracking controllers simultaneously. The parameters of the IRC controller adjusted for the identified model of the plant are:

$$C_t(s) = \frac{418.7}{s}; \quad C_d(s) = \frac{8724}{s}; \quad d = -0.7294 \quad (15)$$

B. PPF Control scheme

The closed-loop poles of the controlled system by means of the PPF control scheme can be adjusted in a fifth-order Butterworth filter pattern to obtain:

$$C_t(s) = \frac{1313}{s} \quad (16)$$

$$C_d(s) = \frac{5.5 \times 10^7}{s^2 + 1.173 \times 10^4 s + 4.856 \times 10^7} \quad (17)$$

C. PVPF Control scheme

The PVPF control scheme can be adjusted to achieve a fifth-order Butterworth filter pattern using:

$$C_t(s) = \frac{2136}{s} \quad (18)$$

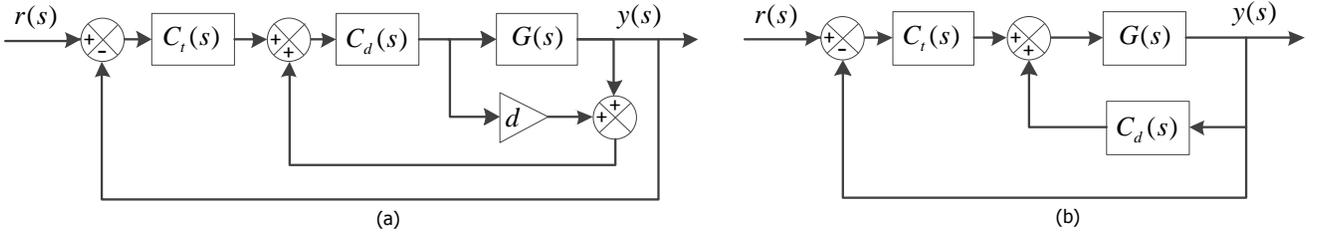$$C_d(s) = \frac{1.504 \times 10^4 s + 6.811 \times 10^7}{s^2 + 1.446 \times 10^4 s + 8.435 \times 10^7} \quad (19)$$

Fig. 4. Block diagram of (a) the IRC, and (b) the PPF/PVPF control schemes where G(s) is the plant, Cd(s) is the damping controller, Ct(s) is the tracking controller, and d is a constant gain, which can be chosen arbitrarily.
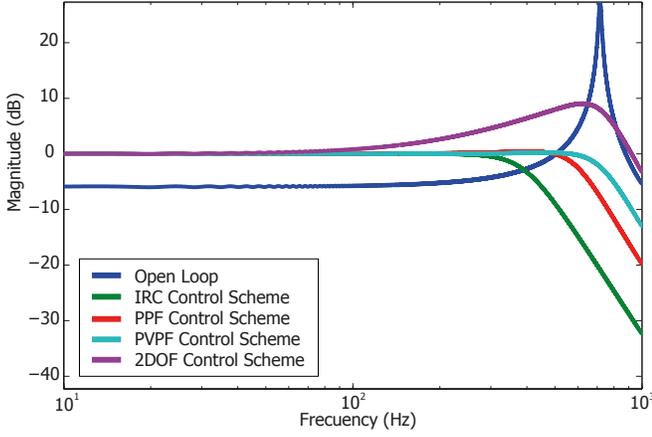

Fig. 5. Magnitude response of the nanopositioning platform, the second order model of the platform, and the simulated closed-loop magnitude response of the traditional and 2DOF-PI^{2}D control schemes.

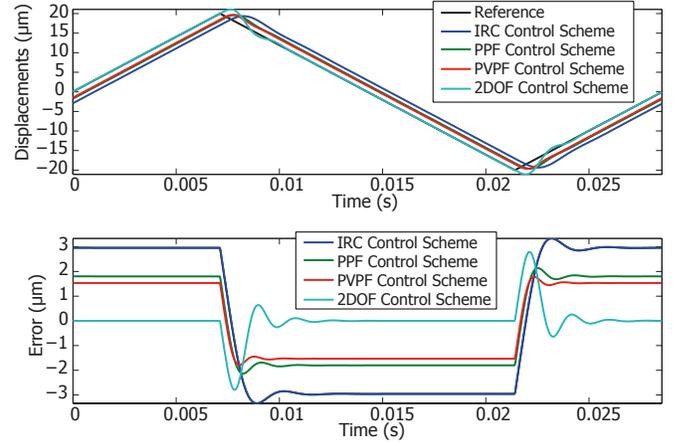| Control scheme	Bandwidth 3 dB (Hz)
IRC	394
PPF	614
PVPF	736.8
2DOF-PI^{2}D	220.8

TABLE I

SIMULATION RESULTS

Fig. 6. Closed-loop system response and error of the different control schemes for a triangular input waveform of frequency, 35 Hz, and amplitude, 20 μm.

D. 2DOF-PI^{2}D Control scheme

When the structure of the 2DOF-PI^{2}D control scheme is utilised to control the system, the closed-loop poles are placed in a sixth-order Butterworth filter pattern and the resulting controllers are:

$$C_t(s) = \frac{2517s + 2.83 \times 10^6}{s^2} \tag{20}$$

$$C_d(s) = \frac{1.11 \times 10^4 s + 6.371 \times 10^7}{s^2 + 1.381 \times 10^4 s + 7.512 \times 10^7} \tag{21}$$

E. Performance comparison

In order to quantify the performance of the different control schemes the 3-dB bandwidth is used as the main criteria. The simulated closed-loop frequency response of all the aforementioned control schemes are presented in Fig. 5 and the achieved bandwidths are tabulated in Table I. Though the 2DOF-PI^{2}D controller delivers a smaller bandwidth than the rest of the controllers, it is the only controller capable of zero-error tracking of ramp-like signals thereby resulting in lesser errors as seen in Fig. 6, where all control schemes are forced to track a triangular signal with a frequency of 35 Hz.

It can be seen from Fig. 6, that only the 2DOF-PI^{2}D controller proposed in this article is capable of zero-error tracking of ramp signals, leading to a superior positioning

performance. Fig. 7 shows the trend of the increase in the root-mean-square error (RMSE) computed for one cycle of triangular signal within a range of frequencies from 0 Hz to 100 Hz, for each of the aforementioned controllers. It is clear that the proposed controller delivers a superior accuracy even at higher frequencies in spite of the relatively lower 3-dB bandwidth.

In the next section, experimental results that validate the superior performance delivered by the proposed control scheme are presented.

VI. EXPERIMENTAL RESULTS

The performance of the proposed controller is evaluated on the two-axis serial kinematic nanopositioner described in Section IV.

A. Time-domain Results

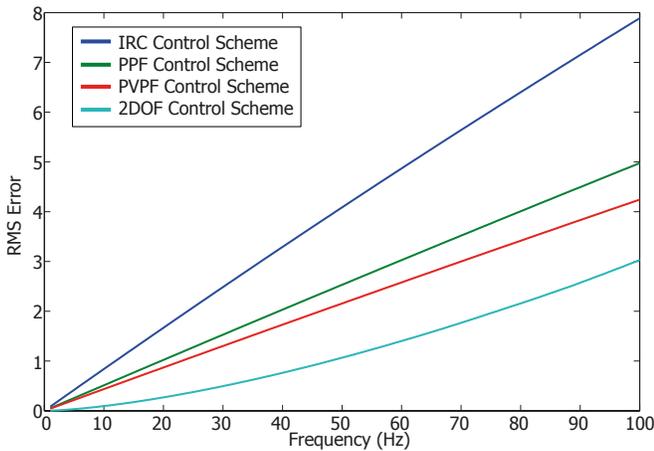To quantify the time-domain performance of each control scheme, the platform is subjected to a triangular input

Fig. 7. RMS Error produced by the the simulated closed-loop response of the traditional, and 2DOF-PI^{2}D control schemes in the tracking of triangular signals of different frequencies
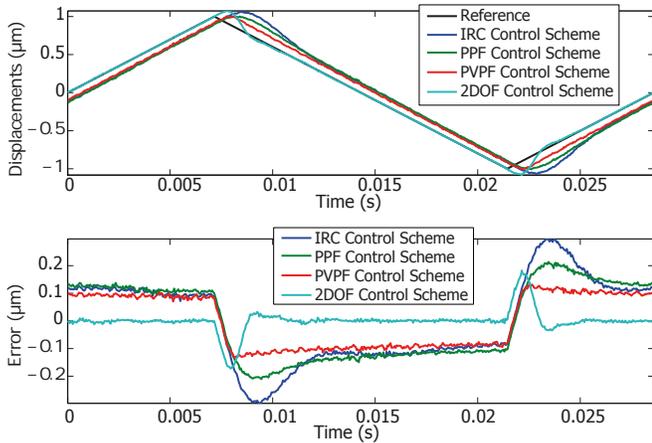

Fig. 8. Experimental closed-loop system response and error of the various control schemes compared, using a triangular input waveform of frequency, 35 Hz, and amplitude, 1 m.

waveform typically employed during raster scan. The applied triangular wave signal has a frequency of 35 Hz and an amplitude of 1 m. The system response and the tracking error are shown in Fig. 8.

Control scheme	Max. Error (m)	RMS Error (m)
IRC	0.297	0.151
PPF	0.214	0.138
PVPF	0.132	0.098
2DOF-PI^{2}D	0.183	0.039

TABLE II

EXPERIMENTAL RESULTS

It can be seen that the experimental results agree well with the simulated results. The 2DOF-PI^{2}D control scheme tracks close to 90% of the linear part of the triangle with zero tracking error. The maximum error (occurring at the corners of the triangle wave) and the RMS error obtained with each controller are showed in Table II.

VII. CONCLUSIONS

In this paper, proposed a new control scheme applicable to nanopositioning systems, capable of tracking ramp and triangular signals with zero steady state error has been proposed. Simulations carried out show that the proposed controller presents a better temporal performance, and produces a much smaller tracking error than other classical control schemes for a wide range of frequencies of the reference triangular signal, thereby delivering a positioning performance with greater accuracy. The control design is simple and explicit equations for controller parameter selection have been derived.

The control scheme's performance has been validated via experimental results, showing that the control methodology developed in this paper yields superior tracking performance for ramp-like scan trajectories popularly used in raster scanning employed in AFMs.

REFERENCES

[1] A.J. Fleming. *Design, Modeling and Control of Nanopositioning Systems*. Advances in industrial control. Springer, 2014.
[2] S. O. Reza Moheimani. Invited review article: Accurate and fast nanopositioning with piezoelectric tube scanners: Emerging trends and future challenges. *Review of Scientific Instruments*, 79(7):–, 2008.
[3] S. Devasia, E. Eleftheriou, and S.O.R. Moheimani. A survey of control issues in nanopositioning. *Control Systems Technology, IEEE Transactions on*, 15(5):802–823, Sept 2007.
[4] A. Sebastian and S.M. Salapaka. Design methodologies for robust nano-positioning. *Control Systems Technology, IEEE Transactions on*, 13(6):868–876, Nov 2005.
[5] Qingsong Xu. Design and development of a compact flexure-based xy precision positioning system with centimeter range. *Industrial Electronics, IEEE Transactions on*, 61(2):893–903, Feb 2014.
[6] Sumeet Aphale, Andrew J Fleming, and S O Reza Moheimani. Integral resonant control of collocated smart structures. *Smart Materials and Structures*, 16(2):439, 2007.
[7] S.S. Aphale, B. Bhikkaji, and S.O.R. Moheimani. Minimizing scanning errors in piezoelectric stack-actuated nanopositioning platforms. *Nanotechnology, IEEE Transactions on*, 7(1):79–90, Jan 2008.
[8] B. Bhikkaji, M. Ratnam, and S.O.R. Moheimani. *f*PVPF*g* control of piezoelectric tube scanners. *Sensors and Actuators A: Physical*, 135(2):700 – 712, 2007.
[9] Douglas Russell, Andrew J. Fleming, and Sumeet S. Aphale. Simultaneous optimization of damping and tracking controller parameters via selective pole placement for enhanced positioning bandwidth of nanopositioners. In *American Control Conference (ACC), 2014*, pages 2184–2189. IEEE, Jun. 2014.
[10] Sachin P Wadikhaye, Yuen Kuan Yong, Bharath Bhikkaji, and S O Reza Moheimani. Control of a piezoelectrically actuated high-speed serial-kinematic afm nanopositioner. *Smart Materials and Structures*, 23(2):025030, 2014.
[11] A.A. Eielsen, M. Vagia, J.T. Gravdahl, and K.Y. Pettersen. Damping and tracking control schemes for nanopositioning. *Mechatronics, IEEE/ASME Transactions on*, 19(2):432–444, April 2014.
[12] K. Ogata. *Modern Control Engineering*. Instrumentation and controls series. Prentice Hall, 2010.
[13] T. McKelvey, H. Akcay, and L. Ljung. Subspace-based multivariable system identification from frequency response data. *Automatic Control, IEEE Transactions on*, 41(7):960–979, Jul 1996.
[14] D. Russell, A. San-Millan, V. Feliu, and S.A. Sumeet. Butterworth pattern based simultaneous damping and tracking controller designs for nanopositioning systems. In *Control Conference (ECC), 2015 European*, July 2015.